Improved estimates of water cycle change from ocean salinity: the key role of ocean warming

Environmental Research Letters

LETTER

Improved estimates of water cycle change from ocean salinity: the key role of ocean warming

Jan D Zika[1,4], Nikolaos Skliris[2], Adam T Blaker[3], Robert Marsh[2], A J George Nurser[3] and Simon A Josey[3]

1 School of Mathematics and Statistics, University of New South Wales, Sydney, Australia
2 University of Southampton, National Oceanography Centre, Southampton, United Kingdom
3 National Oceanography Centre, Southampton, United Kingdom
4 Author to whom any correspondence should be addressed.

E-mail: j.zika@unsw.edu.au

Keywords: water cycle, ocean warming, ocean salinity, climate change

Supplementary material for this article is available online

OPEN ACCESS

RECEIVED
21 March 2018

REVISED
18 June 2018

ACCEPTED FOR PUBLICATION
21 June 2018

PUBLISHED
19 July 2018

Abstract

Changes in the global water cycle critically impact environmental, agricultural, and energy systems relied upon by humanity (Jiménez Cisneros *et al* 2014 *Climate Change 2014: Impacts, Adaptation, and Vulnerability* (Cambridge: Cambridge University Press)). Understanding recent water cycle change is essential in constraining future projections. Warming-induced water cycle change is expected to amplify the pattern of sea surface salinity (Durack *et al* 2012 *Science* **336** 455–8). A puzzle has, however, emerged. The surface salinity pattern has amplified by 5%–8% since the 1950s (Durack *et al* 2012 *Science* **336** 455–8, Skliris *et al* 2014 *Clim. Dyn.* **43** 709–36) while the water cycle is thought to have amplified at close to half that rate (Durack *et al* 2012 *Science* **336** 455–8, Skliris *et al* 2016 *Sci. Rep.* **6** 752). This discrepancy is also replicated in climate projections of the 21st century (Durack *et al* 2012 *Science* **336** 455–8). Using targeted numerical ocean model experiments we find that, while surface water fluxes due to water cycle change and ice mass loss amplify the surface salinity pattern, ocean warming exerts a substantial influence. Warming increases near-surface stratification, inhibiting the decay of existing salinity contrasts and further amplifying surface salinity patterns. Observed ocean warming can explain approximately half of observed surface salinity pattern changes from 1957–2016 with ice mass loss playing a minor role. Water cycle change of 3.6% ± 2.1% per degree Celsius of surface air temperature change is sufficient to explain the remaining observed salinity pattern change.

1. Introduction

Rates of rainfall and evaporation are tightly linked to the vapour pressure of water, which increases by approximately 7% per degree Celsius of warming, raising concerns global warming will substantially enhance the hydrological cycle (Held and Soden 2006). Global climate models project overall increases in evaporation and precipitation, rainfall extremes, and the implied net transport of moisture from net precipitation to net evaporation zones (Durack *et al* 2012, Liu *et al* 2012, Lau *et al* 2013). At regional scale, increased vapour pressure may be compensated by changes in atmospheric circulation (Chadwick *et al* 2013) and subject to influences on evaporation other than warming (Laîné *et al* 2014).

Given limitations in the global network of rainfall measurements (Hegerl *et al* 2015) and substantial discrepancies between atmospheric reanalysis products, model-based reconstructions of past rainfall and water cycle change avoid proper scrutiny and projections of future change are highly uncertain (Schanze *et al* 2010, Skliris *et al* 2014, Levang and Schmitt 2015, Grist *et al* 2016, Yu *et al* 2017). It has been proposed that ocean salinity be used to estimate past water cycle change via its imprint on surface salinity patterns. Net evaporation increases salt concentration, while net precipitation lowers salt concentration. Surface salinity changes are indeed dramatic, with saline regions of the globe becoming more saline and fresh regions becoming more fresh (Durack and Wijffels 2010, figures 1(*a*)–(*c*)).

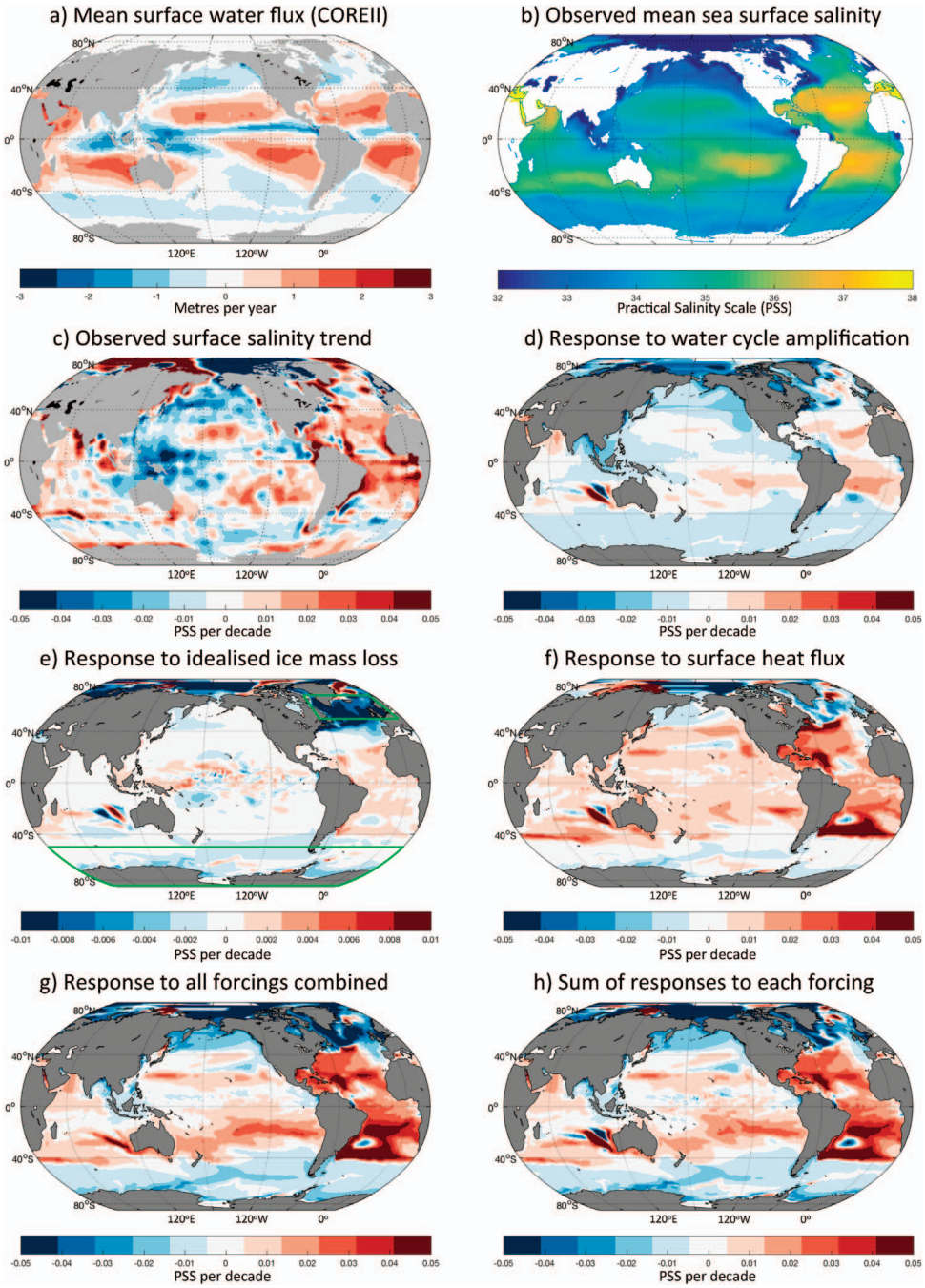

Figure 1. (*a*) Mean fresh water flux out of the ocean from reanalysis data. Mean (*b*) and long term trend (*c*) in sea surface salinity from observational analysis. Simulated sea surface salinity trend over 100 years in response to: (*d*) 1% per decade water cycle amplification; (*e*) idealised water flux anomaly from ice mass loss (water flux anomalies are applied in green boxes); (*f*) 0.2 W m^{-2} per decade surface heat flux anomaly; (*g*) combined water cycle amplification, heat flux and glacial mass loss forcing; and (*h*) sum of responses shown in (*d*)–(*f*). The colour scale for panel (*e*) has been reduced to amplify the small signal in that experiment.

Because surface signals are rapidly advected by ocean currents, salinity measurements at individual locations are not akin to 'rain gauges' (Yu 2011). Full depth salinity observations combined with a three dimensional picture of ocean circulation could provide strong constraints on water cycle change. However subsurface observations remain sparse. Bulk measures of global salinity change, such as salinity pattern amplification (PA hereafter, see methods), can filter out and/or integrate over some of the rearrangement effects caused by variability in ocean currents (Helm *et al* 2010, Durack *et al* 2012, Zika *et al* 2015). PA has been used to infer historical trends in water cycle change (Durack *et al* 2012, Skliris *et al* 2016). However, the relationship between surface salinity pattern changes and water cycle change is puzzling (Vinogradova and Ponte 2017). While the surface salinity pattern has amplified by 5%–8% since 1950 (Durack *et al* 2012, Skliris *et al* 2014), changes in full depth salinity suggest a water cycle change of only 2%–3% (Skliris *et al* 2016). Surface salinity PA also exceeds amplification of the water cycle in climate model projections (Durack *et al* 2012).

To address the above puzzle, we undertake perturbation experiments using a realistic global ocean model. We find that, in addition to water cycle changes and ice mass loss, surface ocean warming is a key and previously overlooked process driving sea surface salinity amplification. We then consider observations of salinity pattern amplification, glacial melt and ocean warming and use these to estimate historical water cycle changes.

2. Data and methods

2.1. Observational data

Observed multi-decadal salinity changes are investigated here using the UK Met Office Hadley Centre Enhanced Ocean Data Assimilation and Climate prediction (ENACT) archive version 4 (EN4, subversion En4.2.2 (Good *et al* 2013)) objectively-analysed monthly dataset covering the 1950–2016 period, at $1° \times 1°$ horizontal grid and a vertical grid of 42 levels.

PA of sea surface salinity is defined as the slope of the linear regression by basin zonal averages of SSS change versus the climatological mean SSS anomaly from the global climatological sea surface salinity (Durack *et al* 2012).

Ocean heat content time series for the upper 2000 m between 1957 and 2016 are obtained from data.nodc.noaa.gov and Boyer *et al* (2013). Although standard error estimates are provided with these, we add an uncertainty of 15% to be consistent with uncertainties in long term ocean heat content change recently reported (e.g. 288 ± 44 ZJ; ZJ = 10^{21} Joules) for the period 1960–2015 (Cheng *et al* 2017). For the ocean deeper than 2000 m and period 1991–2010 an additional 33 ± 22 TW of ocean heat uptake has been reported (Desbruyères *et al* 2016). To create a time series for this deep component we assume there is a linear trend in heat uptake from 1956 reaching 33 PW in the year 2000 and increasing linearly there after. The resulting ocean heat uptake between 1957 and 2016 is 345 ± 75 ZJ in close agreement with recent estimates (e.g. 335 ± 70 ZJ for the period 1960–2010 (Cheng *et al* 2017)).

Church *et al* (2013) document estimates of fresh water input into the ocean for the period 1993–2010 attributed to mass loss from glaciers and the Greenland ice sheet (1.2 ± 0.4 mm yr^{-1}), mass loss from Antarctic ice sheets (0.27 ± 0.11 mm yr^{-1}) and land water storage changes (0.38 ± 0.12 mm yr^{-1}). This fresh water input totals 1.7 ± 0.4 mm yr^{-1} or 19 ± 5 mSv (Sv = 10^6 m^3 s^{-1}). The contrast between estimates of northern and southern hemisphere ice mass loss motivated the 2:1 ratio of fresh water input into the North Atlantic Ocean and Southern Oceans respectively in our ice mass loss numerical ocean modelling experiments discussed below.

An estimate of the rate of multi-year sea-ice mass loss of 3.1 ± 1.0 km decade^{-1} (9.8 ± 3.2 mSv) is obtained from http://psc.apl.uw.edu/research/projects/arctic-sea-ice-volume-anomaly/ and was derived using the method described by Schweiger *et al* (2011). For simplicity, we assume that fresh water input from both land-ice mass loss and sea-ice mass loss increased linearly from zero in 1957 to reported values at the midpoint of their respective observational period (i.e. 2001 for land-ice and 1998 for sea-ice), increasing linearly thereafter.

2.2. Numerical ocean model perturbation experiments

We use NEMO (Nucleus for European Modelling of the Ocean) (Madec 2008) v3.5 in the global ORCA1 configuration. The model grid has a 1° longitudinal resolution at the equator with refined meridional resolution in the tropics transitioning to a tri-polar isotropic mercator grid elsewhere. The model has 75 z coordinate vertical levels increasing in thickness from 1 m at the surface to 250 m in the abyssal ocean. This model configuration is the National Oceanography Centre contribution to a recent model intercomparison project (Danabasoglu *et al* 2014) where it is described in further detail.

The control simulation starts from rest and is integrated for a spin-up period of 400 years. It is then continued for a further 100 years to allow comparison with the control simulation conducted with explicit flux forcing. Surface forcing is provided by CORE-2 normal year forcing (Large and Yeager 2009), interfaced to the model through CORE bulk formulae. Ice is represented by the Louvain-la-Neuve ice model version 2 (LIM2) sea ice model (Timmermann *et al* 2005). Climatological initial conditions for temperature and salinity were taken in January from PHC2.1 (Steele *et al* 2001) at high latitudes, MEDATLAS (Jourdan *et al* 1998) in the Mediterranean, and elsewhere using the *World Ocean Atlas* (Boyer *et al* 2013).

Drift in temperature and salinity is negligible below 1000 m (supplementary figures S1(*a*) and (*b*) available at stacks.iop.org/ERL/13/074036/mmedia). The upper 1000 m shows a gradual warming, which stabilises at 0.7 °C after around 200 years. There is a small surface fresh bias in the upper 200 m, with a saline bias subsurface between 500–800 m. Again these appear stable after 200 years. The mean surface temperature and salinity bias from the EN4 1980–1999 average (figures S1(*c*) and (*d*)) is minimal over most of the global ocean. The largest temperature biases are in the North Atlantic and Nordic Seas. Salinity biases are largest in the Arctic. Rigorous tuning of NEMO ORCA2, forced by the CORE2 normal year, identified a persistent warm bias in the upper ocean which was largest around 200 m depth, and spatial distributions of surface T and S anomalies (similar to those in figure S1), suggesting that the biases may be inherent to the forcing, arise from the use of the EN4 climatology, or are structural to NEMO (Williamson *et al* 2017).

Surface fluxes for the decade spanning years 391 and 400 of the spin-up integration, including those at the base of the ice (surface of the liquid ocean) and those due to the weak salinity restoring, were stored at 6 hourly intervals. The model was then adjusted to remove the interactive ice model and to read surface fluxes directly instead of computing them through the CORE bulk formulae. A 100 year explicit flux forced control experiment, starting at year 391, was then conducted using 10 repeat cycles of this decade of explicit surface fluxes. Although the effect of surface salinity restoring is captured in the saved fluxes from the spin-up, no salinity restoring is used throughout the 100 year control and perturbation experiments.

The difference in drift between the bulk formulae forced and explicit flux forced control simulations is small, with differences in global mean temperature and salinity both in the region of two hundredths of a unit (degree/pss) (figure S1(*e*) and (*f*)). This shows the model to be in a stable state close to equilibrium, and forms the baseline on which to assess heat and water flux anomaly experiments.

Flux anomaly patterns are introduced temporally in two ways: as a step-increase with respect to time (e.g. following Marshall *et al* 2015, Gregory *et al* 2016) and as a linear trend.

Three types of perturbation patterns were added to the saved fluxes to force perturbation experiments: the first was a global amplification of the mean water flux pattern (10% step change and 1%/decade linear trend); the second was a globally constant heat flux anomaly (2 W m^{-2} step change and 0.2 W m^{-2} decade^{-1} linear trend); and the third was an idealised glacial and sea-ice mass loss fresh water flux two thirds of which is distributed over the sub-polar North Atlantic between 50°N and 70°N (i.e. following Stouffer *et al* 2006) and one third of which was evenly distributed south of 50°S (the total flux 0.03 Sv for step change experiment and 0.003 Sv decade^{-1} in the linear trend case).

Our forcing anomaly patterns for water fluxes, surface heat fluxes and glacial and sea-ice mass loss are highly idealised and simplify their complex dynamics. Climate model inter-comparison project (CMIP5) experiments with one per cent per year atmospheric CO_2 radiative forcing increases, show water flux pattern changes qualitatively similar to an amplification of the mean water flux pattern (Gregory *et al* 2016). Warming patterns tend to be associated with larger downward heat fluxes at high latitudes and weaker downward (or even upward heat fluxes) at low latitudes (Gregory *et al* 2016). The latter is likely closely coupled to an individual model's circulation change (Marshall *et al* 2015). We consider our uniform heat flux approach to be useful since it does not assume or force particular ocean circulation changes and is straightforward to reproduce. To our knowledge, there is no consensus on how high latitude ice mass loss will be distributed as the climate warms. Most likely, some will remain near coasts and be influenced by boundary currents while a substantial fraction will likely be distributed further offshore via iceberg drift and melting, as in the present day (Martin and Adcroft 2010, Marsh *et al* 2015). We have chosen our ice mass loss flux strategy so as to maintain simplicity and consistency with other model studies.

In addition we have run an experiment with all three forcings applied (in the linear-trend forcing cases) to the same experiments to assess the linearity of the responses. All data from perturbation experiments shown in the manuscript are deviations from the control experiment.

The above experimental design was inspired by Marshall *et al* (2015). Our approach differs from theirs in the following ways however: (i) in addition to the surface heat flux we also perturb fresh water fluxes; (ii) we do not include any feedbacks between the ocean state and the surface flux (both heat and fresh water flues are explicitly controlled); and (iii) 6 hourly data were used for the explicit flux forced experiments rather than daily data.

3. Results

In water cycle experiments, 1% per decade amplification over 100 years leads to simulated surface salinity changes (figure 1(*d*)) that are qualitatively consistent with the observed pattern of change (figure 1(*c*)). Some differences can be identified, such as freshening in the sub-polar North Atlantic in our model—which is not seen in observations. This region does not appear to conform to the wet gets wetter dry gets dryer paradigm in observations. Some re-analysis products suggest a large increase in net evaporation over the whole North Atlantic and even a reduction in net precipitation over the North Atlantic sub-polar region (Skliris *et al* 2014). Such changes have been associated with Atlantic Multidecadal Variability (Zhang 2017) which we do not account for in our forcing anomalies.

Idealised ice mass loss experiments apply a freshening in the sub-polar North Atlantic (0.002 Sv per decade) and Southern Ocean (0.001 Sv per decade). These led to surface freshening at high latitudes, in particular the North Atlantic, with limited changes at lower latitudes (figure 1(*e*)), the latter likely due to teleconnected changes in ocean circulation.

In warming experiments with surface heat flux anomalies increasing by 0.2 W m^{-2} per decade, surface salinity changes after 100 years (figure 1(*f*)) are also qualitatively similar to that in the water cycle change experiments. Differences are most prominent in the equatorial Pacific where water cycle amplification drives freshening, while warming leads to only a muted response. Furthermore some local changes, such the a patch of freshening at the centre of the South Atlantic, are likely related to a circulation response unique to this model configuration and experimental set-up.

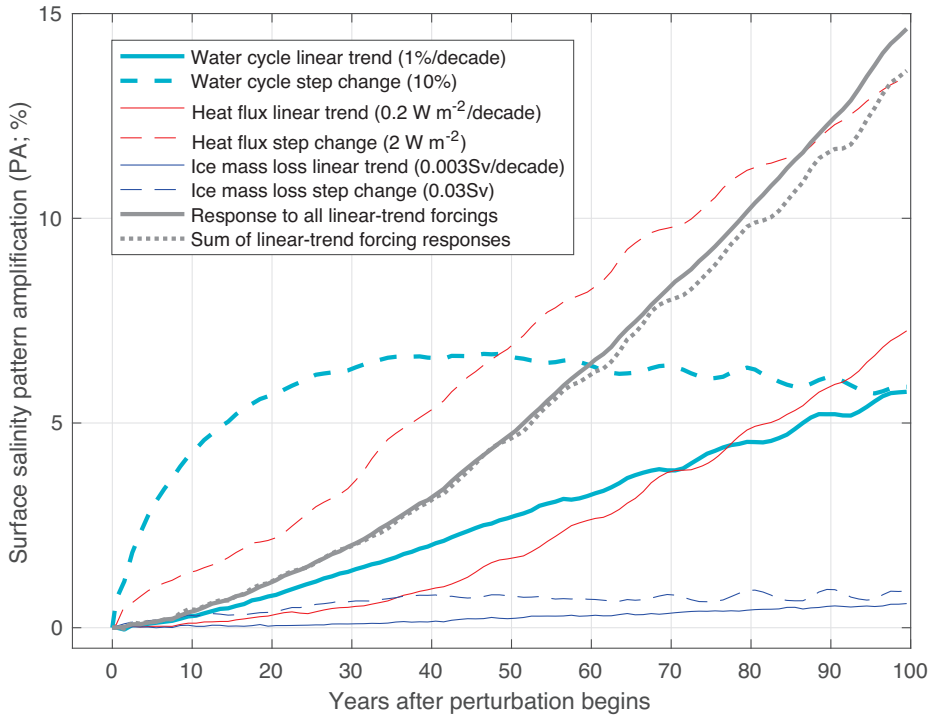

Figure 2. Response of surface salinity pattern amplification (PA; %) to surface forcing changes in numerical ocean model experiments. Shown are responses to amplified water cycle (cyan), uniform anomalous ocean warming (red) and fresh water input from ice mass loss distributed over the sub-polar North Atlantic and Southern Ocean (blue). Solid lines show experiments where fluxes increase linearly with time and dashed lines experiments where fluxes have an abrupt step change. Also shown is the response of the model to the sum of all forcing changes (linear increases; solid grey) and the sum of forcing responses when simulated independently (dotted grey).

We now compare PA per experiment (figure 2). A water cycle trend of 1% per decade yields PA of 5.8% after 100 years. A 10% step change in the water cycle leads to a rapid initial PA adjustment approaching quasi-equilibrium after 40 years at 5.9%. A linear trend in ice mass loss of 0.003 Sv decade^{-1} leads to a linear change in PA reaching 0.6% after 100 years, while a step change of 0.03 Sv per (sub-polar North Atlantic: 0.02 Sv; Southern Ocean: 0.01 Sv) leads to PA of 0.8% which plateaus after 40 years.

Following heat flux linear trends of 0.2 W m^{-2} per decade (figure 2), PA reaches 7.3% after 100 years, indicating considerable PA response to warming. Under a step change warming of 2 W m^{-2}, PA increases monotonically throughout the century, reaching 13.4% at year 100.

The response of surface salinity to these different forcing anomalies is approximately linear. A simulation combining water cycle change, ice mass loss and surface warming forcing anomalies yields approximately the same surface salinity response (figures 1(*g*) and 2) as the sum of the individual simulated responses to each forcing anomaly (figures 1(*h*) and 2). There are regions where the response to warming and fresh water fluxes are not linear. West of Australia is a prime example where a wave like pattern of salinity change is seen. These patterns differ from experiment to experiment and are likely associated with nonlinear circulation processes (such as variability of the Leeuwin Current and meanders of Antarctic Circumpolar Current fronts) which are sensitive to differences in initial and boundary conditions.

The perturbation experiments suggest that, while the surface salinity pattern amplifies with the water cycle, the ratio of PA to water cycle amplification on multi-decadal timescales is less than unity (in terms of % change), in the absence of other forcing anomalies. Ocean warming however drives substantial salinity pattern amplification.

4. Discussion

We now address two outstanding questions: (i) by what mechanism does ocean warming lead to PA?; and (ii) can historical ocean warming plausibly explain a substantial portion of observed PA?

4.1. How does ocean warming lead to salinity pattern amplification?

To address this question, we employ a method based on the water mass framework. Specifically we will consider changes in the distribution of ocean volume as a function of salinity (Zika *et al* 2015). The volume of water contained between surfaces of constant salinity only varies if there are changes in surface water fluxes or changes in mixing. The latter acts in a fairly predictable way, always mixing salt from high to low

salinity regions. In contrast surface salinity is influenced by ocean circulation changes and variability and the effects of ocean mixing on surface salinity are not as straightforward (Yu 2011).

The water mass framework permits a balance to be defined between the rate of change of the mean deviation of salinity over the whole ocean (W; the average deviation of salinity, S, from its global mean, $\bar{S}$) variations in the water cycle F_w , which transports fresh water from saline regions (where $S > \bar{S}$) to fresh regions (where $S < \bar{S}$) and a diffusive flux D which transports salt back from saline to fresh regions (Zika *et al* 2015). This balance is given by

$$\frac{dW}{dt} = \frac{2\bar{S}}{V_0}F_w - \frac{2}{V_0}D \quad (1)$$

where V_0 is the total volume of the ocean. The above equation is exact in the Boussinesq approximation and when there is no net fresh water flux into or out of the ocean (i.e. the total volume of the ocean remains constant) which is the case in our experiments where no water cycle or water flux change is applied. In our control and linearly increasing heat flux anomaly experiments $\bar{S} = 34.72$ pss (this value does not change with the perturbation since the total fresh water flux is identical in both runs). In the final decade of the control experiment $W = 0.18$ pss and in the perturbation W increases by = 0.0021 pss. Although the geographical pattern of water fluxes do not change between these two runs, the pattern of salinity does change, implying different salinity layers are exposed to different fresh water fluxes and hence different rates of fresh water transport from saline to fresh regions. This leads to an increase in F_w of 11 mSv between the control and perturbation.

Using (1) and changes in W and F_w we infer a reduction in D of 8.45×10^2 kg s^{-1} between the control and linearly increasing heat flux experiment. This is equivalent to a fresh water flux anomaly of 24 mSv from saline to fresh regions (i.e. a reduction in the mean fresh water flux due to mixing which is from fresh to saline waters). This change in diffusive flux due to the warming anomaly has the same effect on the full depth salinity contrast (i.e. not only the surface salinity pattern) as an increase in the water cycle of approximately 1% on average over the experiment.

We hypothesise that the reduction in the diffusive flux of fresh water from fresh to saline regions in our warming experiments is at least in part explained by changes in near-surface stratification. Surface warming (figure 3(*a*)) changes surface stratification and thus increases the stability of surface layers. More stable surface stratification inhibits the formation of deep mixed layers and isolates surface salinity anomalies from dilution with the ocean interior (Capotondi *et al* 2012). This hypothesis is corroborated by generally shallower mixed layer depths in warming experiments (figure 3(*c*)).

Salinity can also strongly influence ocean stratification (de Boyer Montégut *et al* 2007). However, in our simulations we find that warming is a far stronger driver of stratification change than water fluxes. For example with and without water flux changes (holding other forcing patterns fixed) we see near negligible differences in surface temperature changes between simulations. The North Atlantic is an exception. There high latitude freshening causes weakening of the AMOC and consequent SST changes (not shown).

4.2. How does ocean warming affect estimates of water cycle change?

Here to attribute observed salinity PA to the three discussed processes (water cycle change, ice mass loss and ocean warming), we use a linear transient response approach (Hasselmann *et al* 1993). Using this approach we can diagnose the time-dependent response of a particular variable (such as PA) based on the time-dependent change in a particular forcing (water cycle change, ice mass loss and warming), using the time-dependent response of the system to step changes in those forcings.

If R_{PA} is the linear transient response (LTR) of PA to a step increase in a specified forcing (F; e.g. the water cycle), then the linear response of PA to time-variable forcing ($F(t)$) follows as:

$$\mathrm{PA}(t) = \int_0^t R_{\mathrm{PA}}(t - t')\frac{dF}{dt'}dt'. \quad (2)$$

Our step change perturbation experiments allow us to diagnose R_{PA} for each forcing: water cycle change; ice mass loss; and surface warming.

A fundamental assumption in the linear transient response approach is that the relationship between forcing effects and their response is linear. We assess this assumption by comparing the linear trend forcing experiment results to predictions made by LTR which exploit output from the step change experiments. That is, we are asking how well can we predict the linear trend response given output from the step change experiments.

Figure S2 shows PA between each linear trend experiment and its LTR reconstruction. The period of interest for our observational reconstruction is between 1958 and 2017 so we will focus on validation of 60 year reconstructions. After 60 years PA for the water cycle amplification experiment matches the LTR reconstruction to within a factor of 0.03 (i.e. PA is 3.22% for the simulation and 3.31% based on LTR). For the ice melt case the difference is a factor 0.1 and in the warming case a factor of 0.12. For all the forcings combined the discrepancy is less than a factor of 0.11.

Using the time series of ocean heat content change discussed in section 2.1, we estimate that ocean warming resulted in a contribution to PA of 2.21% ± 0.46% between 1958 and 2016 (figure 4(*b*)). Estimates of fresh water input into the ocean, comprising both total glacial melt (mass input into the ocean from melting land

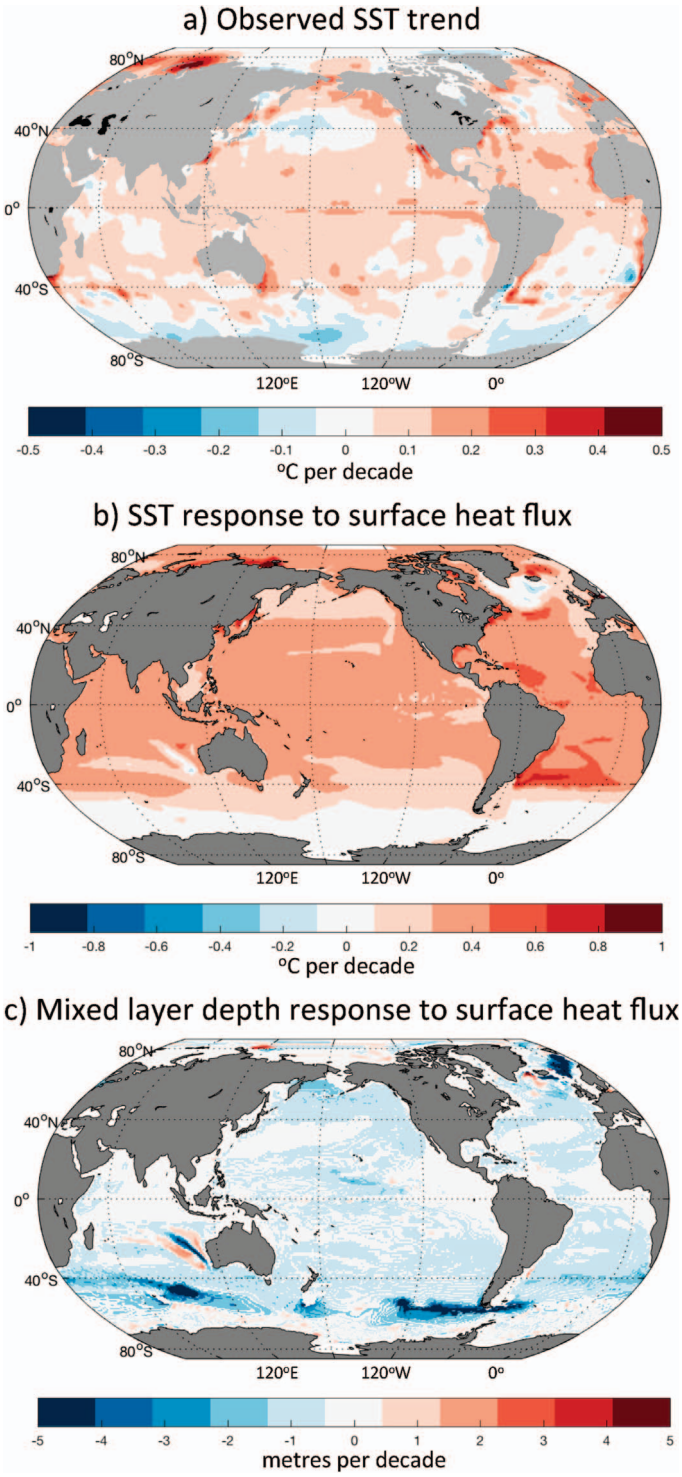

Figure 3. (*a*) Trend in sea surface temperature since 1950 from observational analysis. Simulated trend over 100 years of (*b*) sea surface temperature and (*c*) mixed layer depth in response to an 0.2 W m^{-2} per decade surface heat flux anomaly.

glaciers and ice sheets) and melting of multi-year sea ice, suggest a contribution to PA of 0.75% ± 0.14% up to 2016 (figure 4(*b*)).

We have estimated PA based on the most recent objectively analysed hydrographic observations for periods 1957 to: 1985; 1995; 2005 and 2016. Between 1957 and 2016, the surface salinity pattern amplified by 5% ± 1.1%. Having inferred the contributions to PA from surface ocean warming and ice mass loss, we subtract these from the observed PA up to 2016. The resulting residual PA is 2.04% ± 1.2% over 1957–2016 (figure 4(*b*)), which we attribute to water cycle change.

Observational estimates of water cycle change are unreliable (Hegerl *et al* 2015). Model studies, however, have consistently suggested a tight relationship between measures of water cycle change (e.g. global mean precipitation, meridional moisture transport, etc) and global mean surface air temperature change

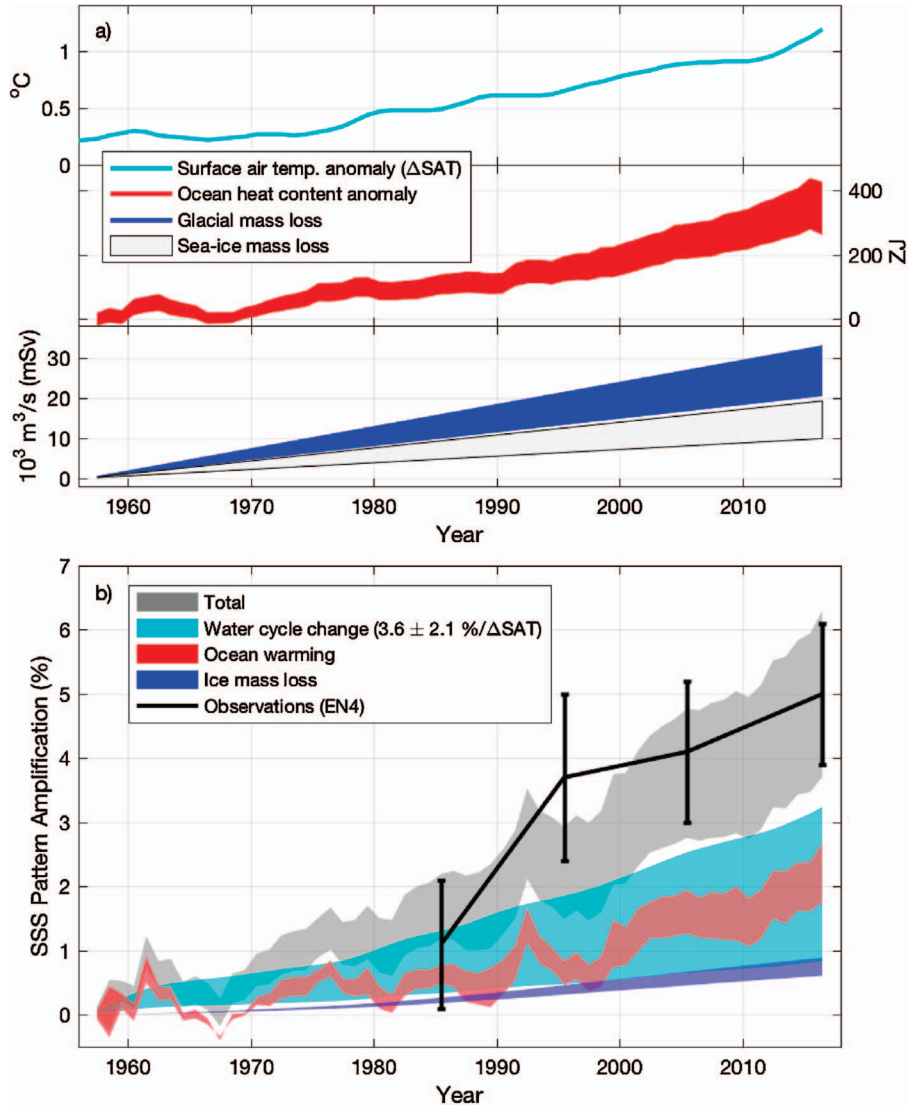

Figure 4. (*a*) Global mean surface air temperature change (ΔSAT) relative to the period 1880–1920 (cyan); five-year running mean global ocean heat content anomaly relative to 1957 (red); ice mass loss from glaciers (blue) and sea-ice (light gray). (*b*) Proposed budget of contributions to salinity pattern amplification including surface warming (red), idealised ice mass loss (blue) and water cycle amplification related linearly to surface air temperature change (cyan). Shown in grey is the sum of these contributions and in black observationally based linear trend estimates (1957–1987, 1957–1995, 1957–2005, 1957–2016).

(ΔSAT; see Kirtman *et al* (2013) and references therein). We thus reduce the problem of quantifying water cycle change to a single multiplying factor for ΔSAT. We use NASA air temperature data (Hansen *et al* 2010) and note that uncertainties in global air temperature are negligible compared to the range of possible water cycle to SAT amplification factors. Combining the transient linear response approach and the water cycle forced PA inferred above and the ΔSAT time-series we infer an amplification factor of 3.6% ± 2.1% per degree Celsius ΔSAT.

Our 60 year PA estimate based on EN4 is weaker than 50 year estimates from recent authors (5.4% Boyer *et al* (2005), 5.5% Hosoda *et al* (2009), and 8% Durack *et al* (2012)). Linearly extrapolating those three estimates to 60 years and weighting them equally with our EN4 based estimate yields PA of 6.9% ± 1.9%. Subtracting the effect of ocean warming and ice mass loss, as above, the implied amplification factor is 6.9 ± 3.6%/°C. Analysis by Durack *et al* (2012) was distinct in that trends estimated in regions where data coverage was substantial were extrapolated to regions where data coverage was not sufficient to discern a trend. Conversely in other analyses, which used optimal interpolation or objective analysis, trends were only estimated, and therefore contributed to PA, close to regions where observations supported a trend. Excluding Durack *et al*'s estimate yields an amplification factor of 5.4 ± 0.18%/°C and considering only their estimate and reported uncertainty (0.7%) yields an amplification of 11.6 ± 1.7%/°C.

5. Conclusions

Surface salinity observations have previously been put forward as a means to estimate past water cycle amplification and monitor ongoing variability and change

(Schmitt 2008, Kerr *et al* 2010). Our analysis suggests a strong influence of ocean warming on the evolution of surface salinity. In numerical simulations with anomalous surface warming we have shown that the surface salinity pattern amplifies substantially. This change is coincident with a reduction in the diffusive flux of fresh water from fresh to saline waters and reduced mixed layer depths. There is potential for water cycle changes to be monitored using surface salinity observations if these surface warming effects are appropriately accounted for.

Combining both numerical model experiments and observational analysis up to 2016 we report that approximately one third of observed salinity pattern amplification can be explained by ocean warming and one sixth by ice mass loss. The remaining signal can be attributed to a water cycle amplification of 3.6% ± 2.1% per degree Celsius of global surface air temperature rise.

Acknowledgments

This research was supported by the Natural Environment Research Council (NERC) through the Atlantic Climate System Integrated Study (ACSIS; grant NE/N018044/1) and the Australian Research Council (ARC; grant DP160103130).

ORCID iDs

Jan D Zika https://orcid.org/0000-0003-3462-3559

References

Boyer T P, Levitus S, Antonov J, Locarnini R and Garcia H 2005 Linear trends in salinity for the world ocean, 1955–98 *Geophys. Res. Lett.* **32** L01604

Boyer T P *et al* 2013 *World Ocean Database 2013* (NOAA Printing Office)

Capotondi A, Alexander M A, Bond N A, Curchitser E N and Scott J D 2012 Enhanced upper ocean stratification with climate change in the CMIP3 models *J. Geophys. Res. Oceans* **117** C04031

Chadwick R, Boutle I and Martin G 2013 Spatial patterns of precipitation change in CMIP5: why the rich do not get richer in the tropics *J. Clim.* **26** 3803–22

Cheng L, Trenberth K E, Fasullo J, Boyer T, Abraham J and Zhu J 2017 Improved estimates of ocean heat content from 1960–2015 *Sci. Adv.* **3** e1601545

Church J *et al* 2013 Section 13 *Sea Level Change* (Cambridge: Cambridge University Press) pp 1137–216

Danabasoglu G *et al* 2014 North Atlantic simulations in coordinated ocean-ice reference experiments phase II (core-II). Part I: mean states *Ocean Model.* **73** 76–107

de Boyer Montégut C, Mignot J, Lazar A and Cravatte S 2007 Control of salinity on the mixed layer depth in the world ocean: 1. general description *J. Geophys. Res. Oceans* **112** C06011

Desbruyères D G, Purkey S G, McDonagh E L, Johnson G C and King B A 2016 Deep and abyssal ocean warming from 35 years of repeat hydrography *Geophys. Res. Lett.* **43** 19

Durack P J and Wijffels S E 2010 Fifty-year trends in global ocean salinities and their relationship to broad-scale warming *J. Clim.* **23** 4342–62

Durack P J, Wijffels S E and Matear R J 2012 Ocean salinities reveal strong global water cycle intensification during 1950–2000 *Science* **336** 455–8

Good S A, Martin M J and Rayner N A 2013 EN4: quality controlled ocean temperature and salinity profiles and monthly objective analyses with uncertainty estimates *J. Geophys. Res. Oceans* **118** 6704–16

Gregory J M *et al* 2016 The flux-anomaly-forced model intercomparison project (FAFMIP) contribution to CMIP6: investigation of sea-level and ocean climate change in response to CO_2 forcing *Geosci. Model Dev.* **9** 3993

Grist J P, Josey S A, Zika J D, Evans D G and Skliris N 2016 Assessing recent air-sea freshwater flux changes using a surface temperature-salinity space framework *J. Geophys. Res. Oceans* **121** 8787–806

Hansen J, Ruedy R, Sato M and Lo K 2010 Global surface temperature change *Rev. Geophys.* **48**

Hasselmann K, Sausen R, Maier-Reimer E and Voss R 1993 On the cold start problem in transient simulations with coupled atmosphere-ocean models *Clim. Dyn.* **9** 53–61

Hegerl G C *et al* 2015 Challenges in quantifying changes in the global water cycle *Bull. Am. Meteorol. Soc.* **96** 1097–115

Held I M and Soden B J 2006 Robust responses of the hydrological cycle to global warming *J. Clim.* **19** 5686–99

Helm K P, Bindoff N L and Church J A 2010 Changes in the global hydrological-cycle inferred from ocean salinity *Geophys. Res. Lett.* **37** 18

Hosoda S, Suga T, Shikama N and Mizuno K 2009 Global surface layer salinity change detected by Argo and its implication for hydrological cycle intensification *J. Oceanogr.* **65** 579–86

Jiménez Cisneros B E, Oki T, Arnell N W, Benito G, Cogley J G, Döll P, Jiang T and Mwakalila S S 2014 Freshwater Resources *Climate Change 2014: Impacts, Adaptation, and Vulnerability* vol 1 (Cambridge: Cambridge University Press) ch 3 pp 229–69

Jourdan D, Balopoulos E, Garcia-Fernandez M-J and Maillard C 1998 Objective analysis of temperature and salinity historical data set over the Mediterranean Basin *OCEANS'98 Conf. Proc.* vol 1 (IEEE) pp 82–7 (see ieee.org or https://ieeexplore.ieee.org/stamp/stamp.jsp?tp=&arnumber=726257)

Kerr Y H *et al* 2010 The SMOS mission: a new tool for monitoring key elements of the global water cycle *Proc. IEEE* **98** 666–87

Kirtman B *et al* 2013 Section 11 *Near-term Climate Change: Projections and Predictability* (Cambridge: Cambridge University Press) pp 953–1028

Laîné A, Nakamura H, Nishii K and Miyasaka T 2014 A diagnostic study of future evaporation changes projected in CMIP5: climate models *Clim. Dyn.* **42** 2745–61

Large W and Yeager S 2009 The global climatology of an interannually varying air–sea flux data set *Clim. Dyn.* **33** 341–64

Lau W K-M, Wu H-T and Kim K-M 2013 A canonical response of precipitation characteristics to global warming from CMIP5: models *Geophys. Res. Lett.* **40** 3163–9

Levang S J and Schmitt R W 2015 Centennial changes of the global water cycle in CMIP5 models *J. Clim.* **28** 6489–502

Liu C, Allan R P and Huffman G J 2012 Co-variation of temperature and precipitation in CMIP5: models and satellite observations *Geophys. Res. Lett.* **39** 13

Madec G 2008 NEMO ocean engine *Note du Pole de modelisation, Institut Pierre-Simon Laplace (IPSL), France, 27*

Marsh R *et al* 2015 NEMO–ICB (v1. 0): interactive icebergs in the NEMO ocean model globally configured at eddy-permitting resolution *Geosci. Model Dev.* **8** 1547

Marshall J, Scott J R, Armour K C, Campin J-M, Kelley M and Romanou A 2015 The ocean's role in the transient response of climate to abrupt greenhouse gas forcing *Clim. Dyn.* **44** 2287–99

Martin T and Adcroft A 2010 Parameterizing the fresh-water flux from land ice to ocean with interactive icebergs in a coupled climate model *Ocean Model.* **34** 111–24

Schanze J J, Schmitt R W and Yu L 2010 The global oceanic freshwater cycle: a state-of-the-art quantification *J. Mar. Res.* **68** 569–95

Schmitt R W 2008 Salinity and the global water cycle *Oceanography* **21** 12–9

Schweiger A, Lindsay R, Zhang J, Steele M, Stern H and Kwok R 2011 Uncertainty in modeled Arctic sea ice volume *J. Geophys. Res. Oceans* **116** c00D06

Skliris N, Marsh R, Josey S A, Good S A, Liu C and Allan R P 2014 Salinity changes in the world ocean since 1950 in relation to changing surface freshwater fluxes *Clim. Dyn.* **43** 709–36

Skliris N, Zika J D, Nurser G, Josey S A and Marsh R 2016 Global water cycle amplifying at less than the Clausius-Clapeyron rate *Sci. Rep.* **6** 752

Steele M, Morley R and Ermold W 2001 PHC: a global ocean hydrography with a high-quality Arctic ocean *J. Clim.* **14** 2079–87

Stouffer R J *et al* 2006 Investigating the causes of the response of the thermohaline circulation to past and future climate changes *J. Clim.* **19** 1365–87

Timmermann A, Goosse H, Madec G, Fichefet T, Ethe C and Dulire V 2005 On the representation of high latitude processes in the ORCA-LIM global coupled sea-ice ocean model *Ocean Model.* **8** 175–201

Vinogradova N T and Ponte R M 2017 In search of fingerprints of the recent intensification of the ocean water cycle *J. Clim.* **30** 5513–28

Williamson D B, Blaker A T and Sinha B 2017 Tuning without over-tuning: parametric uncertainty quantification for the NEMO ocean model *Geosci. Model Dev.* **10** 1789

Yu L 2011 A global relationship between the ocean water cycle and near-surface salinity *J. Geophys. Res. Oceans* **116** C10025

Yu L, Jin X, Josey S A, Lee T, Kumar A, Wen C and Xue Y 2017 The global ocean water cycle in atmospheric reanalysis, satellite, and ocean salinity *J. Clim.* **30** 3829–52

Zhang R 2017 On the persistence and coherence of subpolar sea surface temperature and salinity anomalies associated with the Atlantic multidecadal variability *Geophys. Res. Lett.* **44** 7865–75

Zika J D, Skliris N, Nurser A G, Laliberte F, Mudryk L, Josey S and Marsh R 2015 Maintenance and broadening of the ocean's salinity distribution by the water cycle *Geophys. Res. Lett.* **42** 4940–8